The Seismic Record
A journal of the Seismological Society of America

The Far Side of Mars: Two Distant Marsquakes Detected by InSight

Anna C. Horleston* *et al.*

Abstract

For over three Earth years the Marsquake Service has been analyzing the data sent back from the Seismic Experiment for Interior Structure—the seismometer placed on the surface of Mars by NASA's InSight lander. Although by October 2021, the Mars seismic catalog included 951 events, until recently all these events have been assessed as lying within a radius of 100° of InSight. Here we report two distant events that occurred within days of each other, located on the far side of Mars, giving us our first glimpse into Mars' core shadow zone. The first event, recorded on 25 August 2021 (InSight sol 976), shows clear polarized arrivals that we interpret to be *PP* and *SS* phases at low frequencies and locates to Valles Marineris, 146° ± 7° from InSight. The second event, occurring on 18 September 2021 (sol 1000), has significantly more broadband energy with emergent *PP* and *SS* arrivals, and a weak phase arriving before *PP* that we interpret as P_{diff}. Considering uncertain pick times and poorly constrained travel times for P_{diff}, we estimate this event is at a distance between 107° and 147° from InSight. With magnitudes of M_w^{Ma} 4.2 and 4.1, respectively, these are the largest seismic events recorded so far on Mars.

Cite this article as Horleston, A. C., Clinton, J. F., Ceylan, S., Giardini, D., Charalambous, C., Irving, J. C. E., Lognonné, P., Stähler, S. C., Zenhäusern, G., Dahmen, N. L., et al. (2022). The Far Side of Mars: Two Distant Marsquakes Detected by InSight, *The Seismic Record*. **2**(**2**), 88–99, doi: 10.1785/0320220007.

Supplemental Material

Introduction

For the past three years or ~1100 sols, the Marsquake Service (MQS) has been analyzing the data recorded by the Seismic Experiment for Interior Structure (SEIS; Lognonné *et al.*, 2019) as part of the National Aeronautics and Space Administration's InSight mission to Mars (Banerdt *et al.*, 2020). This is the first dedicated geophysics mission to another planet, and the lander carries not only the seismometer package but also atmospheric sensors (Banfield *et al.*, 2019) to fully characterize the local meteorology and the impact of the weather on the seismic records.

MQS (Clinton *et al.*, 2018), an international team of seismologists, performs daily manual analysis of the data, detecting, locating, and cataloging the seismicity in as near-real time as the data downlink rate allows (Clinton *et al.*, 2021). Martian seismic data are generally more complicated than Earth data (Ceylan *et al.*, 2021) due to the surface deployment of SEIS on low-rigidity materials that are deformed by wind-generated forces (Kenda *et al.*, 2020; Lognonné *et al.*, 2020) and the proximity of the lander. In the most recently released catalog extending up to 01 October 2021, the MQS had cataloged 951 marsquakes (InSight Marsquake Service, 2022). These are classified into different types dependent on their frequency content. A broad resonance at 2.4 Hz, excited both during marsquakes as well as by the ambient noise (Dahmen *et al.*, 2021), thought to be due to local subsurface structure (Hobiger *et al.*, 2021), is the key to discriminating between event types.

Marsquakes that have significant long-period energy reaching out to 10 s are considered to be similar to teleseismic earthquakes. They are regularly observed with impulsive and polarized arrivals that match expected body wave arrival times for direct mantle-traversing *P* and *S* phases on Mars (e.g., event S0173a [Marsquakes are labeled by mission sol and a letter to

Full author list and affiliations appear at the end of this article.

*Corresponding author: Anna.Horleston@bristol.ac.uk

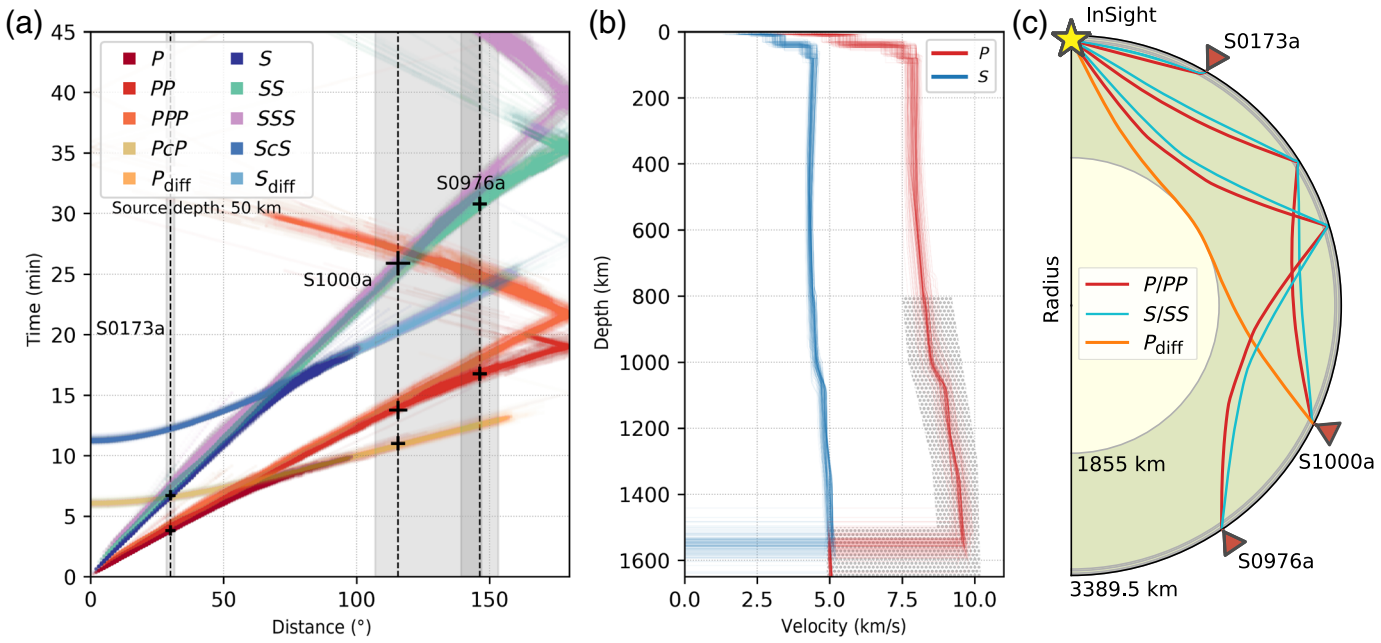

Figure 1. Summary of Martian interior models from Stähler *et al.* (2021) and ray paths for seismic phases from events presented in this article. (a) The travel time curves are computed using the TauP package (Crotwell *et al.*, 1999) for a source depth of 50 km. The phase picks that the Marsquake Service (MQS) identified for these events are indicated with crosses, with varying symbol sizes to schematically reflect the pick uncertainties. The distant events are S1000a and S0976a. For comparison, also shown is S0173a, an event at 30° that locates at Cerberus Fossae. For all three events, high-amplitude phase arrivals have been identified as direct *P/S* for S0173a and single free-surface reflections *PP/SS* for S1000a and S0976a. For S1000a, a weak P_{diff} phase that is diffracted along the core–mantle boundary is also identified. The vertical dashed lines and gray shaded bars mark the event distances and uncertainties from Table S1, respectively. (b) The structural models are not constrained by observations for depths below ~800 km for *P* waves (hatched region; Khan *et al.*, 2021), hence the P_{diff} travel times are purely from model predictions. (c) Illustrates the ray paths of the identified phases using a Mars model with a core radius of 1855 km.

distinguish between multiple events in a sol] in Fig. 1). MQS conventions divide this family into low-frequency (LF) and broadband (BB) events; the latter type also includes seismic excitation at and above the 2.4 Hz resonance. A second family of events have high-frequency energy dominantly at and above 2.4 Hz, also with two distinct phases that are interpreted as trapped crustal phases, and labeled as *Pg* and *Sg*. This event family includes high frequency (HF) and very high frequency (VF) types; the latter having strong horizontal energy up to and exceeding 10 Hz.

Recent studies that use InSight observations provide direct seismological constraints on the size and composition of the Martian core, and the thickness of the crust and mantle (Khan *et al.*, 2021; Knapmeyer-Endrun *et al.*, 2021; Stähler *et al.*, 2021; Durán *et al.*, 2022). A suite of velocity models has been derived from these results, as summarized in Figure 1. At present, lower mantle *P* velocities are not constrained by direct seismic observations. The most recent MQS catalog (InSight Marsquake Service, 2022) provides the epicentral distance for all LF and BB events derived using these new velocity model suites (previous catalogs used models derived prior to landing, see Clinton *et al.*, 2021).

Magnitudes for all event types are estimated using a set of calibrated Mars magnitude scales (Böse *et al.*, 2021). A preferred Mars moment magnitude, M_w^{Ma}, is assigned to each event—for LF family events this is based on the long-period spectral plateau of the *S* wave. Prior to sol 976, all marsquakes locate to less than 75° epicentral distance from InSight from their *S*–*P* differential travel time and have magnitudes below $M_w^{Ma} = 3.8$. A small number of marsquakes have been identified that cannot be located because phases are not clearly *P* and *S*, but they have longer than normal coda durations, suggesting that they are more distant than the well-located events (Clinton *et al.*, 2021).

Direct *P* and *S* waves enter into the core shadow at a distance of ~100°. Beyond this distance, the earliest major body phase arrivals are *PP* and *SS* (Fig. 1a). Once in the shadow for the direct *P* wave, *PP* may be preceded by P_{diff}.

Despite the development of single-station event-location techniques (Khan *et al.*, 2016; Böse *et al.*, 2017), determining the back azimuth for weak teleseisms that exhibit high scattering is challenging. Of the 951 events cataloged, only a small subset have known azimuths, and the majority of these cluster around the Cerberus Fossae fault system at approximately 30° distance from InSight (Giardini *et al.*, 2020; Clinton *et al.*, 2021).

The two new events we present here, S0976a (Fig. 2) and S1000a (Fig. 3), are the largest LF family events detected to date and the first to be located beyond the postulated start of the core shadow zone. Using standard MQS analysis tools (Clinton *et al.*, 2021), we show how the events are characterized. The MQS typically identifies candidate events using an initial screening of sol-long spectrograms (e.g., Fig. 2a). The waveform data are then studied, and the possible events are evaluated in detail. A comodulation analysis between atmospheric and seismic data (Charalambous *et al.*, 2021) is used to aid discrimination between ambient weather-related noise and seismic energy. Comodulation compares the observed broadband seismic energy with predicted broadband seismic energy using the pressure and weather signals, or, if these channels are not available, energy in the lander modes at 4 and 6 Hz that are highly sensitive to winds (Dahmen *et al.*, 2021). To identify onset of phase arrivals, spectrograms and filter banks are used in addition to time series analysis. To aid in phase association and discriminate between *P* and *S* phases, polarization analysis provides information on degree of ellipticity and inclination angle. Once phases are assigned, locations are provided using the aforementioned suite of velocity models, and the polarization of the initial *P* wave is used to provide a back azimuth.

At the time of the S0976a and S1000a events, due to power constraints arising from the steady accumulation of dust on the solar panels, only a limited set of sensors were recording continuously, including the very broadband (VBB) seismic sensor. The short-period (SP) seismometer, and the Temperature and Wind for InSight (TWINS) wind sensors were off. The pressure sensor was recording during S0976a but was off during S1000a.

In this article, we present the S0976a and S1000a events in detail, and discuss the implications of detecting these two distant marsquakes.

Marsquake S0976a

Sol 976 (Fig. 2) was a key day for InSight on Mars, with two significant marsquakes. S0976a—an M_w^{Ma} 4.2-magnitude LF event at ∼146° ± 7° distance from InSight—occurred in the early hours during steady winds typical for this time of day. A few hours later, in the late afternoon, a very noisy time characterized by wind gusts, this was followed by S0976b—an M_w^{Ma} 4.1-magnitude VF event at ∼16°—the highest magnitude event of this class.

S0976a, origin time 25 August 2021 03:32:20 UTC (sol 976 02:26:28 local mean solar time [LMST]), has energy between 1 and 8 s period, and is visible in the time domain on all three components, despite the comparatively high background noise. A prominent, wind-driven lander mode (Dahmen *et al.*, 2021) is evident in the spectrogram in Figure 2 at 4 Hz. However, the seismic signal from the event is visible within the spectrogram and the filterbank (Fig. S1, available in the supplemental material to this article), and is distinct from the atmospheric noise predicted at the time by the pressure sensor (Fig. S2). Energy from the seismic event lasts for approximately an hour—one of the longest duration Martian seismic events observed so far. The event energy is rather narrow-banded across the entire duration, with a peak at 5 s in all components (Fig. 4). As is standard for LF family events, two clear energy pulses can be identified, with the second being the largest. The pulse arrival times are separated by approximately 14 min. Assuming the two arrivals are the main primary and secondary phases, these are assigned as *PP* and *SS* (Fig. 2) based on the Martian velocity models (Fig. 1). This assignment is further supported by the polarization inclination angles of the phases, the first being vertically inclined, supporting *PP*, whereas the second is more horizontally inclined, hence *SS* (Fig. S3). The *PP* phase includes energy between 2 and 6 s, whereas the *SS* phase is both higher in amplitude and wider in frequency, extending from 1 to 8 s (Fig. 4; Fig. S1).

PP can be identified in the time domain, in this analysis, using a 2–6 s band-pass filter with an uncertainty of ± 10 s. Similarly, the *SS* phase is picked in the time domain with ± 10 s uncertainty, using a 2–8 s band-pass filter (Table S1).

Using the velocity models from Stähler *et al.* (2021) (Fig. 1), the *SS*–*PP* time gives a distance of 146° ± 7°. The back azimuth is determined to be 101° ± 25° from the particle motion observed in the first few seconds of the *P*-wave arrival (see Fig. 2d). Combining the azimuth with the distance gives this event an approximate location of 10° S, 78° W. This places the event within the region of Valles Marineris (Fig. 5).

Marsquake S1000a

Figure 3a shows the daily spectrogram for sol 1000. The signal for event S1000a is clearly observed shortly after midnight.

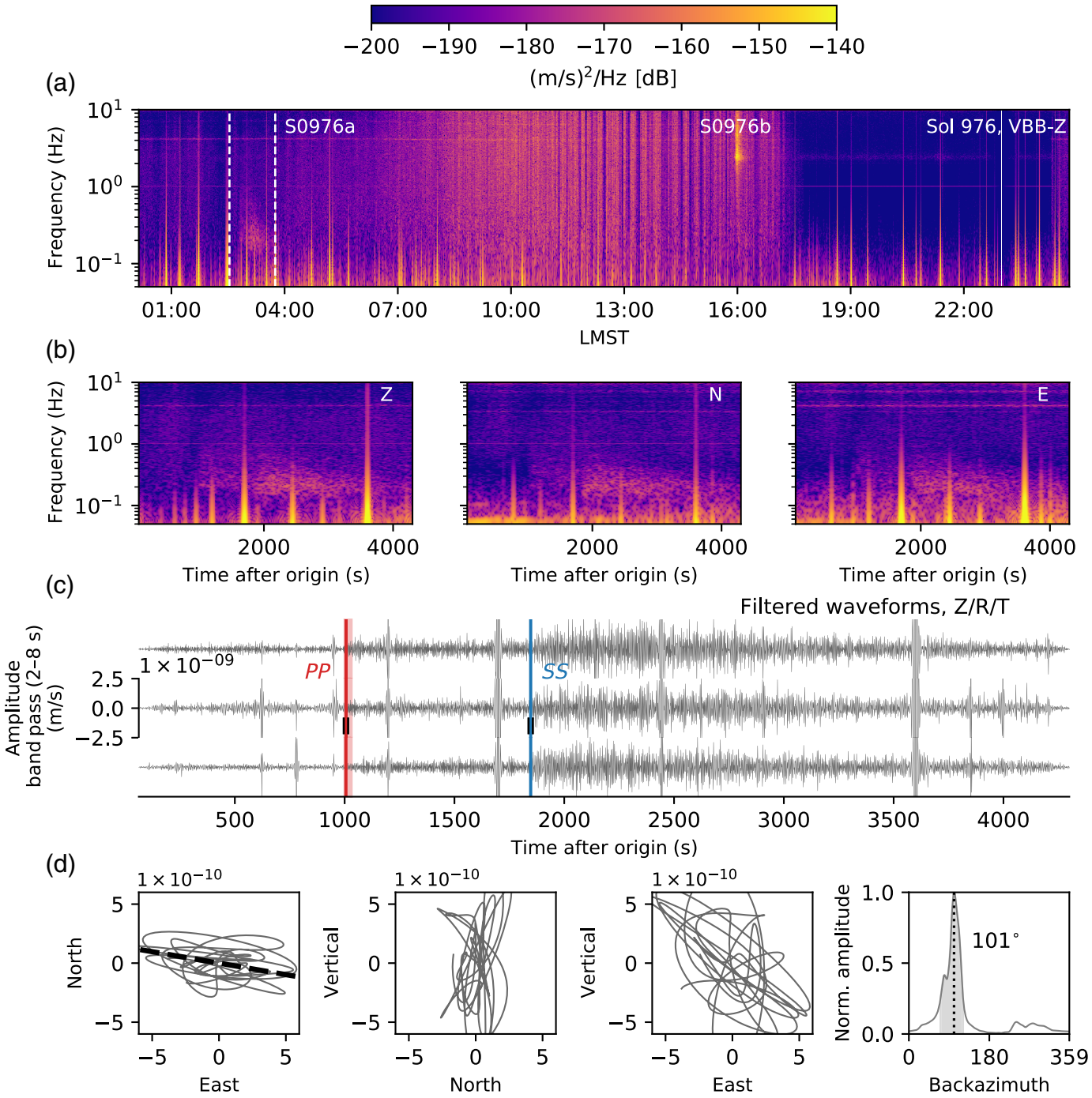

Figure 2. Overview of S0976a. (a) Sol-long velocity spectrogram for 20 samples/s very broadband (VBB) vertical component computed with a window length of 120 s and 50% overlap. The origin and signal end times are marked by vertical white dashed lines. A second event (S0976b, very high frequency [VF]) is also labeled. High-amplitude yellow transient spikes in all spectrograms are glitches or donks; the horizontal feature at 1 Hz (also referred to as *tick noise*) is an artefact from the electronics box measurement system (e.g., Ceylan *et al.*, 2021). Other horizontal features during the windy periods are the lander modes at, for example, 4 Hz, and the 2.4 Hz resonance, which is observed consistently during the quiet evening period. (b) velocity spectrograms for each VBB component (Z, N, and E) focused around the event as marked in panel (a). (c) VBB velocity waveforms filtered between 2 and 8 s, and rotated toward the source (Z, R, and T). The vertical red and blue lines denote the *PP* and *SS* picks, respectively, with uncertainties marked by black error bars. The pink box around the *PP* pick indicates the time window used to create the hodograms in panel (d) for back azimuth determination. (d) Also includes the back azimuth probability density function with 2σ errors marked in gray shade.

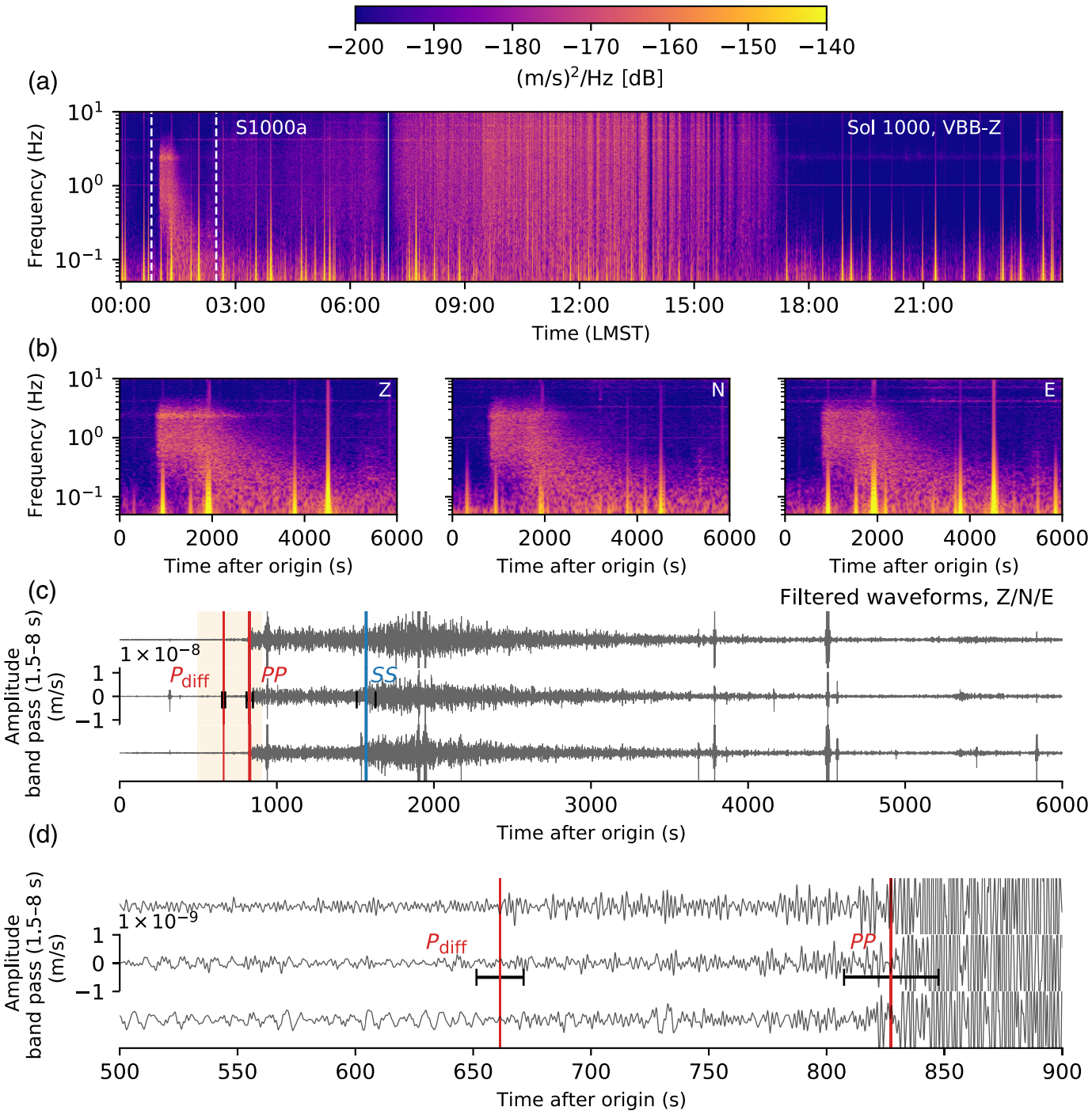

Figure 3. Overview of S1000a. (a) Sol-long velocity spectrogram (window length 120 s with 50% overlap) for 20 samples/s VBB vertical component. The event is marked with dashed vertical lines in the early hours from the origin time to signal end as identified by the MQS. (b) The three-component velocity spectrograms around the S1000a event for the time period as marked in panel (a). (c) Band-pass filtered (1.5–8 s) waveforms. The seismic phase picks of the MQS are shown with vertical lines as labeled. The horizontal error bars indicate the picking uncertainties. (d) A zoom into the waveforms marked with the tan colored box in panel (c).

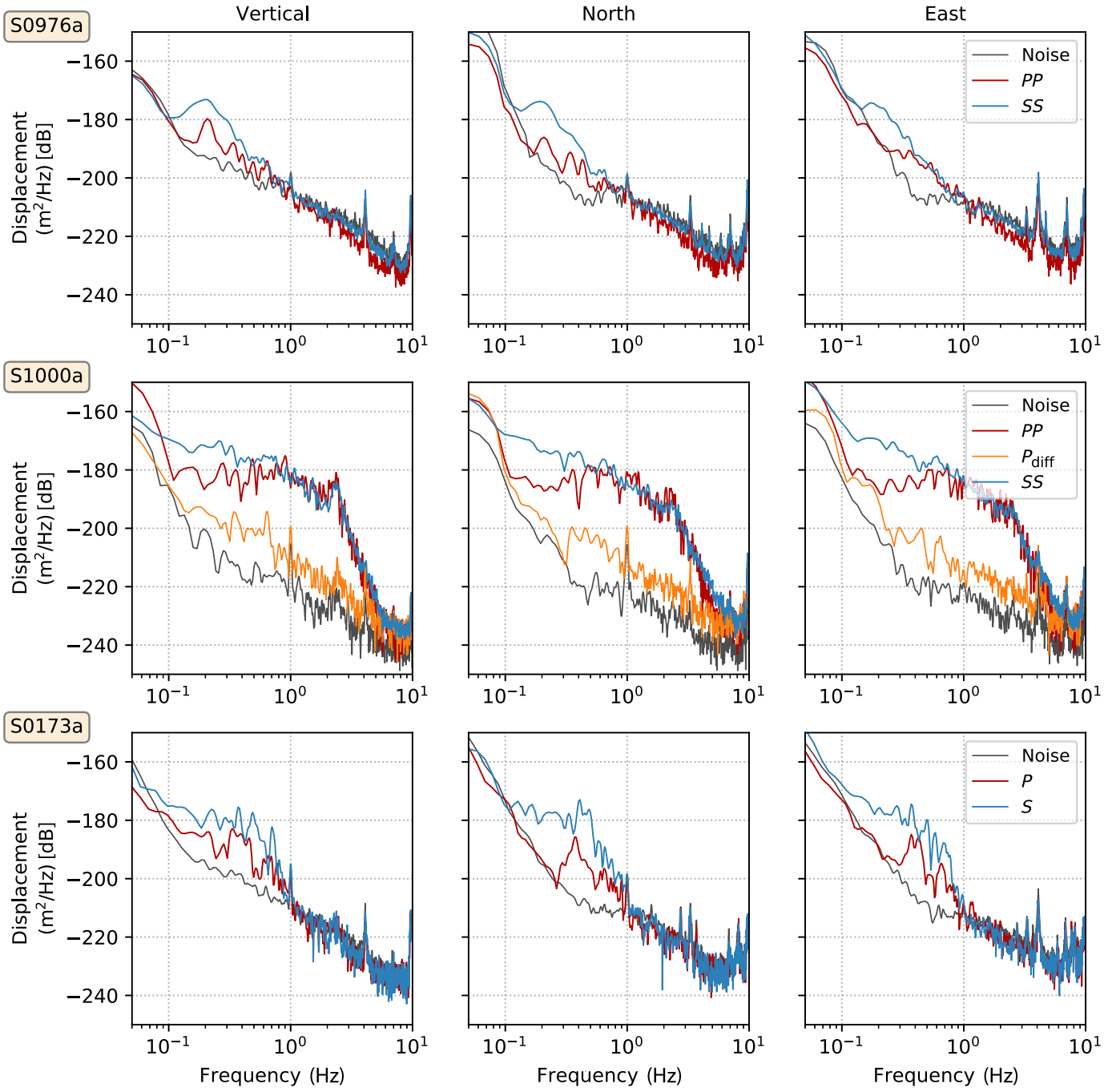

Figure 4. Spectral comparison of events S0976a and S1000a with S0173a—a more typical low-frequency (LF) event that occurred approximately 30° away from InSight, located at Cerberus Fossae. The spectra for S0976a is narrower in frequency content than S0173a but similar in shape with a stronger *SS* phase, particularly at lower frequencies. S1000a also shows a divergence between the *SS* and *PP* at lower frequencies. The vertical spectra for S1000a shows the excess excitation around 2.4 Hz. All the spectra show spikes at the lander resonances, particularly at ~4 and ~7 Hz. The background noise level was particularly low for S1000a, aiding the detection of the low-amplitude P_{diff} phase. All spectra are computed from a ~60 to ~120 s manually selected time window using Welch's method with window length of 30 s and overlap of 50%.

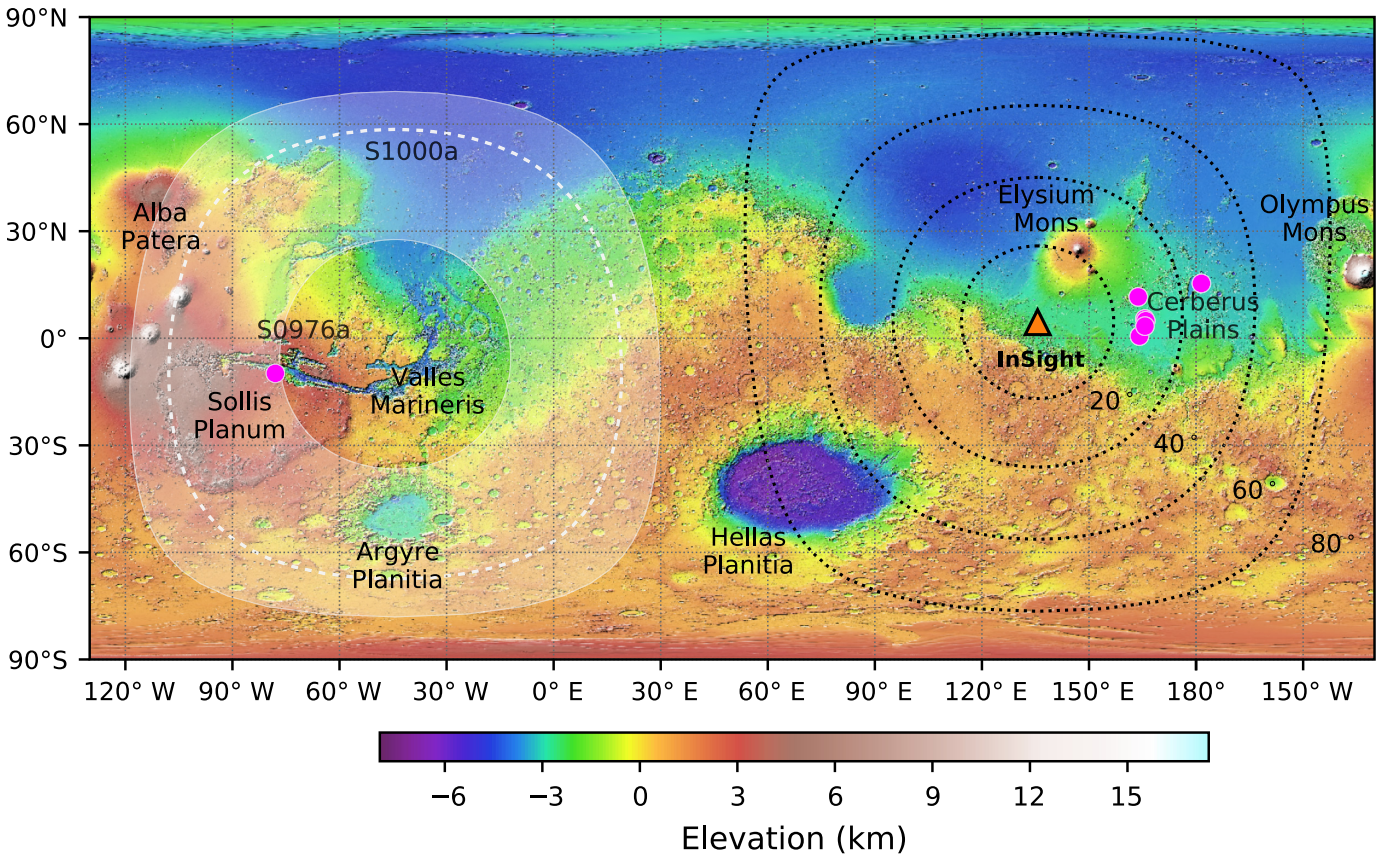

Figure 5. Mars seismicity location map. Mars surface relief map showing InSight's location (orange triangle), the location of other located marsquakes (magenta dots) that cluster around 30° distance, close to Cerberus Fossae, and S0976a, located within Valles Marineris just north of Sollis Planum. Because no back azimuth can be determined for S1000a, its location is predicted to be somewhere within the shaded region between 107° and 147° from InSight. The event's preferred distance (116°) is marked with the white dashed line. The black dotted lines mark radii around InSight up to 80°. The background image is from the Mars Orbiter Laser Altimeter (Smith *et al.*, 2001).

This event is striking in that it has energy from 0.1 to 5 Hz (Fig. 4; Fig. S5)—by far the broadest frequency content of any marsquake observed so far. Although some broadband marsquakes contain high-frequency energy, S1000a is uniquely rich in this energy across a wide band of high frequencies. The MQS categorizes this event as a broadband event with unusually significant high-frequency content and has made picks following the standard procedures (Clinton *et al.*, 2021).

The event origin is estimated at 18 September 2021 17:48:00 UTC (sol 1000 00:48:25 LMST) and lasts for 94 min—the longest event recorded so far on Mars. At higher frequencies the event duration is significantly shorter; the lowest periods extend the duration (Fig. S6). Like S0976a, there are two clear energy pulses, here separated by over 12 min. The earlier phase is richest at highest frequencies, whereas the later phase has more energy at longer periods. Above 1 Hz, the earlier arrival has the largest amplitudes, whereas below, the second phase is far stronger. As in the case of S0976a, considering the large difference in arrival times, the body phases are interpreted as *PP* and *SS*.

The *PP* phase is complicated, with high-frequency energy arriving seconds in advance of the energy below 1 Hz—the frequency in which MQS usually selects *P*-wave arrivals. Though the phase can be identified in the time domain with a 1–100 s band-pass filter, MQS assigns it at 18:01:47 UTC with a wide uncertainty of ± 20 s. *SS* is more emergent and, as is often the case for LF family marsquakes, it is picked using the spectrogram and the filterbank (Fig. S5) at 18:14:08 UTC ± 60 s. The fact that both the *PP* and *SS* phases are complicated is likely due to crustal and lithospheric complexity at the bounce point (also observed on Earth, e.g., Shearer, 1991). Careful analysis of the signal before the clear *P* phase indicates that there is an additional weak phase close to 3 min earlier,

with an onset that can also be identified in the time domain (Fig. 3d; Fig. S5). This phase is only seen at long periods below 1 Hz and is not as complicated—it is identified at 17:59:01 ± 10 s UTC in the time domain with a 2–6 s filter. Like the *PP* arrival, this weaker phase also has a vertical inclination (Fig. S7), whereas the *SS* shows horizontal inclination. Considering the early, vertically polarized arrival for an event with large *SS*–*PP* time, this phase is consistent with P_{diff}—a *P* wave that diffracts along the core–mantle boundary. This assignment is further supported when tested with the probabilistic location algorithms of Böse *et al.* (2017). It is the first time in the mission that such a phase has been seen. Further analyses of the attributes of this P_{diff} signal are in progress.

As is standard for broadband marsquakes, which regularly exhibit time-separated arrivals at different frequencies (Clinton *et al.*, 2021), MQS has also picked phase arrivals for the high-frequency energy within the event between 2.2 and 2.8 Hz. These phases are labeled as y1 and y2 in the marsquake catalog (InSight Marsquake Service, 2022), and are picked at 18:00:57 ± 5 s and 18:14:08 ± 60 s, respectively, the former being 50 s prior to *PP*, the latter coincident with *SS*.

Using P_{diff}, *PP*, and *SS*, the event locates to a distance of 116° ± 9°. If the P_{diff} phase is not included, the event locates to a distance of 128° ± 19°. This surprisingly large variation in distance and uncertainty can be explained by the uncertainty in the phase picks. Because *SS* has a ± 60 s uncertainty, a very broad range of distances are compatible. Once a P_{diff} pick with uncertainty of only ± 10 s is included, this phase has a dominating influence on the preferred distance and reduces the uncertainty in epicentral distance. It is notable that the P_{diff} ray path dives down to the core and hence samples depths that are not well constrained in the velocity models used for the inversion (Fig. 1). The preferred distance reported in this article as well as the corresponding MQS catalog is 116°, derived using all three picks, though here we assign a wider uncertainty from 107° to 147°, reflecting the unclear *SS*-phase arrival and location based on *PP* and *SS* only.

Because of the complexity and emergent nature of the *PP* phase, no back azimuth can be determined and so the locus of potential origins is plotted on Figure 5. The P_{diff} phase, with low signal to noise, also cannot be used to infer polarization.

Similarly to S0976a there are glitches and donks—broadband one-sided signals caused by thermal stress relaxation in the lander, tether or sensor assembly (Scholz *et al.*, 2020)—throughout the event coda (Table S3). These are evident as high-amplitude spikes within the spectrograms shown in Figure 3 and can be seen in Figure S8d within the raw and deglitched acceleration timeseries (see Scholz *et al.*, 2020, for the deglitching methods).

Within the time window of S1000a, a second broadband event, S1000b, potentially an aftershock, is observed. This is a much lower amplitude signal, and it is not possible to pick body phases. The energy of this event is evident within the filterbanks in Figure S5 at around 4500 s and is particularly prominent at 1/2.8 and 1/4 Hz.

Discussion

With these two events, we have our first look into the core shadow zone of Mars; yet these events tell very different stories. Table S1 summarizes the key features of the two events.

The most striking difference between them is their frequency content (Fig. 4). S0976a shows no energy above 1 Hz, yet S1000a includes energy up to 5 Hz. S0976a is similar to many other LF marsquakes observed so far during the mission, for example S0173a—one of the earliest and, prior to sol 976, the largest marsquake detected. In contrast, the high-frequency content in S1000a is unique. The *SS* spectrum of S1000a requires very low intrinsic shear attenuation and high values of mantle Q_{shear} compared to those reported in Giardini *et al.* (2020). The lower frequency content of S0976a may suggest a significantly slower rupture speed than for S1000a.

The disparity in high-frequency content is also reflected in the event magnitudes. Mars magnitudes are calculated following Böse *et al.* (2021). Both the events have similar moment magnitudes, $M^{Ma}_{w,spec}$, with S0976a being slightly larger. $M^{Ma}_{w,spec}$ is based on the seismic moment derived from A_0—the long-period plateau of the *S*-wave displacement spectra (Fig. 4). In contrast, the body wave magnitudes for each of the *P* (m^{Ma}_{bP}) and *S* waves (m^{Ma}_{bS}), based on peak velocity amplitudes between 0.2 and 0.5 Hz, have larger differences, with S1000a being larger (Table S1). It is noted that the spectral magnitude scale $M^{Ma}_{w,spec}$ in Böse *et al.* (2021) is derived using body wave energy from synthetics that extend out to 150°, so it is valid for these extended distances. m^{Ma}_{bP} and m^{Ma}_{bS}, however, are cross calibrated using marsquake data and only for distances observed at the time (<100°), and are therefore not taking all effects of *SS* or *PP* into account. Yet, they allow for a comparison of S0976a and S1000a, which are at similar teleseismic distances.

The location of S0976a is striking. Previous locatable marsquakes have all clustered around Cerberus Fossae—a 10 Ma old graben system ~1500 km east of the lander that is not particularly remarkable when viewed on a global scale. S0976a,

however, locates to Valles Marineris—one of the most significant surface structures on Mars and one of the largest graben systems in the solar system. Kumar *et al.* (2019) predicted seismic activity based on orbital images of fresh boulder falls, landslides, and young crosscutting faults; yet this event is the first confirmed to be at this distance and back azimuth. S0976a will be further studied in this context, and will hopefully shed light on these potential processes and the seismogenic potential of Valles Marineris.

Though S1000a is not fully locatable due to the lack of clear polarization on the *PP* and P_{diff} arrivals, it is still significant that this event locates on the distant hemisphere. The distance of 107°–147° excludes a source region near the large volcano Olympus Mons. Potential sources from geological mapping (Tanaka *et al.*, 2014) could be the extensive graben systems west of Alba Patera that cross basaltic plains of Amazonian age (younger than 600 Ma). Farther south are older terrains, including the western part of Valles Marineris and regions of extensive faulting in Sollis Planum.

The unusually broad frequency spectrum and the amplitude of the S1000a waveforms brings into question the source mechanism of this quake. In many ways it is similar to other HF events in the catalog with prominent excess excitation at 2.4 Hz, and the dominant high frequencies in the *PP* and y1 phases. The coda is slow to decay, and it is possible that this event occurs at much shallower depths than previously recorded for broadband events, thus more energy is trapped within surface-fractured layers, as described in van Driel *et al.* (2021), Karakostas *et al.* (2021), and Menina *et al.* (2021), for example.

Prior to S0976a, the most distant marsquake calculated from *S-P* travel times was at ~72° (Khan *et al.*, 2021). A further handful of events were located by envelope alignment (Giardini *et al.*, 2020) out to roughly the edge of Mars' shadow zone but with no definitive distance assignment. It was thought that the small magnitude of marsquakes may have been a limiting factor to observing distant quakes, but the detection of these two events shows that distant quakes can be seen by InSight, and these quakes will be used to refine the alignments now we have anchor points beyond ~72°.

Seismology has revealed that the core–mantle boundary is a complex region on both the Earth and the Moon (e.g., Weber *et al.*, 2011; Lay, 2015); the observation of, the albeit weak, P_{diff} may provide insights into Mars's core–mantle boundary. Although the initial MQS analysis did not show other phases, for example, S_{diff}, it is likely that with more advanced analysis other new phases will soon be identified within the coda of these events, providing further refinement of our velocity models and greater constraints on crust, mantle, and core structure.

S0976a and S1000a are remarkable events in the Martian seismic catalog, and they will be instrumental in furthering our understanding of the red planet.

Data and Resources

The InSight seismic event catalog version 9 (InSight Marsquake Service, 2022), the waveform data and station metadata are available from the Institut de Physique du Globe de Paris (IPGP) Datacenter and Incorporated Research Institutions for Seismology Data Management Center (IRIS-DMC; http://dx.doi.org/10.18715/SEIS.INSIGHT.XB_2016), as are the previous catalog versions. Seismic waveforms are also available from the National Aeronautics and Space Administration Planetary Data System (NASA PDS, https://pds.nasa.gov/ (http://doi.org/10.17189/1517570). All websites were last accessed in April 2022. The supplemental material includes other key figures used by the Marsquake Service (MQS) in analyzing these events.

Declaration of Competing Interests

The authors acknowledge that there are no conflicts of interest recorded.

Acknowledgments

The authors acknowledge National Aeronautics and Space Administration (NASA), Centre national d'études spatiales (CNES), their partner agencies and Institutions (United Kingdom Space Agency [UKSA], Swiss Space Office [SSO], Deutsches Zentrum für Luft- und Raumfahrt [DLR], Jet Propulsion Laboratory [JPL], Institut de Physique du Globe de Paris [IPGP]-Centre National de la Recherche Scientifique [CNRS], Eidgenössische Technische Hochschule Zürich [ETHZ], Imperial College, London [IC], Max Planck Institute for Solar System Research [MPS-MPG]), and the flight operations team at JPL, Seismic Experiment for Interior Structure (SEIS) on Mars Operation Center (SISMOC), Mars SEIS package data service (MSDS), Incorporated Research Institutions for Seismology Data Management Center (IRIS-DMC) and NASA Planetary Data System (PDS) for providing Standard for Exchange of Earthquake Data (SEED) SEIS data. The InSight event catalog (comprising all events, including phase picks until October 2021) and waveform data are available from the IRIS-DMC, NASA-PDS, SEIS-InSight data portal, and IPGP data center (InSight Marsquake Service, 2022; InSight Mars SEIS Data Service, 2019b, 2019a). Anna C. Horleston, Jessica C. E. Irving,

and Nicholas A. Teanby are funded by the UKSA under Grant Numbers ST/R002096/1, ST/W002523/1, and ST/W002515/1. Nikolaj L. Dahmen, Cecilia Duran, Géraldine Zenhäusern, and Simon C. Stähler would like to acknowledge support from Eidgenössische Technische Hochschule (ETH) through the ETH + funding scheme (ETH+02 19-1: "Planet Mars"). The French coauthors acknowledge the funding support provided by CNES and the Agence Nationale de la Recherche (ANR-19-CE31-0008-08 MAGIS) for SEIS operation and SEIS Science analysis. Alexander E. Stott acknowledges the French Space Agency CNES and ANR (ANR-19-CE31-0008-08). Caroline Beghein and Jiaqi Li were supported by NASA InSight Participating Scientist Program (PSP) Grant Number 80NSSC18K1679. This article is InSight Contribution Number 236.

References

Banerdt, W. B., S. E. Smrekar, D. Banfield, D. Giardini, M. Golombek, C. L. Johnson, P. Lognonné, A. Spiga, T. Spohn, C. Perrin, *et al.* (2020). Initial results from the InSight mission on Mars, *Nature Geosci.* **13,** no. 3, 183–189.

Banfield, D., J. A. ManfrediRodriguez-, C. T. Russell, K. M. Rowe, D. Leneman, H. R. Lai, P. R. Cruce, J. D. Means, C. L. Johnson, A. Mittelholz, *et al.* (2019). InSight auxiliary payload sensor suite (APSS), *Space Sci. Rev.* **215,** no. 1, 1–33.

Böse, M., J. F. Clinton, S. Ceylan, F. Euchner, M. van Driel, A. Khan, D. Giardini, P. Lognonné, and W. B. Banerdt (2017). A probabilistic framework for single-station location of seismicity on Earth and Mars, *Phys. Earth Planet. In.* **262,** 48–65.

Böse, M., S. C. Stähler, N. Deichmann, D. Giardini, J. Clinton, P. Lognonné, S. Ceylan, M. van Driel, C. Charalambous, N. Dahmen, *et al.* (2021). Magnitude scales for marsquakes calibrated from insight data, *Bull. Seismol. Soc. Am.* **111,** no. 6, 3003–3015.

Ceylan, S., J. F. Clinton, D. Giardini, M. Böse, C. Charalambous, M. van Driel, A. Horleston, T. Kawamura, A. Khan, G. Orhand-Mainsant, *et al.* (2021). Companion guide to the marsquake catalog from InSight, Sols 0–478: Data content and non-seismic events, *Phys. Earth Planet. In.* **310,** 106597, doi: 10.1016/j.pepi.2020.106597.

Charalambous, C., A. E. Stott, W. T. Pike, J. B. McClean, T. Warren, A. Spiga, D. Banfield, R. F. Garcia, J. Clinton, S. Stähler, *et al.* (2021). A comodulation analysis of atmospheric energy injection into the ground motion at InSight, Mars, *J. Geophys. Res.* **126,** no. 4, e2020JE006538, doi: 10.1029/2020JE006538.

Clinton, J., D. Giardini, M. Böse, S. Ceylan, M. van Driel, F. Euchner, R. F. Garcia, S. Kedar, A. Khan, S. C. Stähler, *et al.* (2018). The Marsquake service: Securing daily analysis of SEIS data and building the Martian seismicity catalogue for InSight, *Space Sci. Rev.* **214,** no. 8, 1–33.

Clinton, J. F., S. Ceylan, M. van Driel, D. Giardini, S. C. Stähler, M. Böse, C. Charalambous, N. L. Dahmen, A. Horleston, T. Kawamura, *et al.* (2021). The Marsquake catalogue from InSight, sols 0–478, *Phys. Earth Planet. In.* **310,** 106595, doi: 10.1016/j.pepi.2020.106595.

Crotwell, H. P., T. J. Owens, and J. Ritsema (1999). The TauP Toolkit: Flexible seismic travel-time and ray-path utilities, *Seismol. Res. Lett.* **70,** no. 2, 154–160.

Dahmen, N. L., G. Zenhäusern, J. F. Clinton, D. Giardini, S. C. Stähler, S. Ceylan, C. Charalambous, M. van Driel, K. J. Hurst, S. Kedar, *et al.* (2021). Resonances and lander modes observed by InSight on Mars (1–9 Hz), *Bull. Seismol. Soc. Am.* **111,** no. 6, 2924–2950.

Durán, C., A. Khan, S. Ceylan, G. Zenhäusern, S. Stähler, J. Clinton, and D. Giardini (2022). Seismology on Mars: An analysis of direct, reflected, and converted seismic body waves with implications for interior structure, *Phys. Earth Planet. Int.* **325,** 106851, doi: 10.1016/j.pepi.2022.106851.

Giardini, D., P. Lognonné, W. B. Banerdt, W. T. Pike, U. Christensen, S. Ceylan, J. F. Clinton, M. van Driel, S. C. Stähler, M. Böse, *et al.* (2020). The seismicity of Mars, *Nature Geosci.* **13,** no. 3, 205–212.

Hobiger, M., M. Hallo, C. Schmelzbach, S. Stähler, D. Fäh, D. Giardini, M. Golombek, J. Clinton, N. Dahmen, G. Zenhäusern, *et al.* (2021). The shallow structure of Mars at the InSight landing site from inversion of ambient vibrations, *Nat. Commun.* **12,** no. 1, 1–13.

InSight Mars SEIS Data Service (2019a). InSight SEIS Data Bundle, *PDS Geosciences (GEO) Node, ETHZ, IPGP, JPL, ICL, ISAE-Supaero, MPS, Univ. Bristol*, doi: 10.17189/1517570.

InSight Mars SEIS Data Service (2019b). SEIS raw data, InSight Mission, *IPGP, JPL, CNES, ETHZ, ICL, MPS, ISAE-Supaero, LPG, MFSC*, doi: 10.18715/SEIS.INSIGHT.XB_2016.

InSight Marsquake Service (2022). Mars Seismic Catalogue, InSight Mission; V9 2022-01-01, *ETHZ, IPGP, JPL, ICL, ISAE-Supaero, MPS, Univ. Bristol.*, doi: 10.12686/a14.

Karakostas, F., N. Schmerr, R. Maguire, Q. Huang, D. Kim, V. Lekic, L. Margerin, C. Nunn, S. Menina, T. Kawamura, *et al.* (2021). Scattering attenuation of the Martian interior through codawave analysis, *Bull. Seismol. Soc. Am.* **111,** no. 6, 3035–3054.

Kenda, B., M. Drilleau, R. Garcia, T. Kawamura, N. Murdoch, N. Compaire, P. Lognonné, A. Spiga, R. Widmer-Schnidrig, P. Delage, *et al.* (2020). Subsurface structure at the InSight Landing site from compliance measurements by seismic and meteorological experiments, *J. Geophys. Res.* **125,** e2020JE006387, doi: 10.1029/2020JE006387.

Khan, A., S. Ceylan, M. van Driel, D. Giardini, P. Lognonné, H. Samuel, N. C. Schmerr, S. C. Stähler, A. C. Duran, Q. Huang, *et al.* (2021). Upper mantle structure of Mars from InSight seismic data, *Science* **373,** no. 6553, 434–438.

Khan, A., M. van Driel, M. Böse, D. Giardini, S. Ceylan, J. Yan, J. Clinton, F. Euchner, P. Lognonné, N. Murdoch, *et al.* (2016). Single-station and single-event marsquake location and inversion for structure using synthetic Martian waveforms, *Phys. Earth Planet. In.* **258,** 28–42.

Knapmeyer-Endrun, B., M. P. Panning, F. Bissig, R. Joshi, A. Khan, D. Kim, V. Lekić, B. Tauzin, S. Tharimena, M. Plasman, *et al.* (2021). Thickness and structure of the Martian crust from InSight seismic data, *Science* **373,** no. 6553, 438–443.

Kumar, P. S., N. Krishna, K. Lakshmi Prasanna, S. Raghukanth, A. Dhabu, and T. Platz (2019). Recent seismicity in Valles Marineris, Mars: Insights from young faults, landslides, boulder falls and possible mud volcanoes, *Earth Planet. Sci. Lett.* **505,** 51–64.

Lay, T. (2015). 1.22—Deep earth structure: Lower Mantle and D, in *Treatise on Geophysics*, Second Ed., G. Schubert (Editor), Elsevier, Oxford, 683–723.

Lognonné, P., W. B. Banerdt, D. Giardini, W. T. Pike, U. Christensen, P. Laudet, S. Raucourtde, P. Zweifel, S. Calcutt, M. Bierwirth, *et al.* (2019). SEIS: Insight's seismic experiment for internal structure of Mars, *Space Sci. Rev.* **215,** no. 1, 12.

Lognonné, P., W. B. Banerdt, W. T. Pike, D. Giardini, U. Christensen, R. F. Garcia, T. Kawamura, S. Kedar, B. Knapmeyer-Endrun, L. Margerin, *et al.* (2020). Constraints on the shallow elastic and anelastic structure of Mars from InSight seismic data, *Nature Geosci.* **13,** no. 3, 213–220.

Menina, S., L. Margerin, T. Kawamura, P. Lognonné, J. Marti, M. Drilleau, M. Calvet, N. Compaire, R. Garcia, F. Karakostas, *et al.* (2021). Energy envelope and attenuation characteristics of high-frequency (HF) and very-high-frequency (VF) Martian events, *Bull. Seismol. Soc. Am.* **111,** no. 6, 3016–3034.

Scholz, J.-R., R. Widmer-Schnidrig, P. Davis, P. Lognonné, B. Pinot, R. F. Garcia, K. Hurst, L. Pou, F. Nimmo, S. Barkaoui, *et al.* (2020). Detection, analysis, and removal of glitches from InSight's seismic data from Mars, *Earth Space Sci.* **7,** no. 11, e2020EA001317, doi: 10.1029/2020EA001317.

Shearer, P. M. (1991). Constraints on upper mantle discontinuities from observations of long period reflected and converted phases, *J. Geophys. Res.* **96,** no. B11, 18,147–18,182.

Smith, D. E., M. T. Zuber, H. V. Frey, J. B. Garvin, J. W. Head, D. O. Muhleman, G. H. Pettengill, R. J. Phillips, S. C. Solomon, H. J. Zwally, *et al.* (2001). Mars Orbiter laser altimeter: Experiment summary after the first year of global mapping of Mars, *J. Geophys. Res.*, **106,** no. E10, 23,689–23,722.

Stähler, S. C., A. Khan, W. B. Banerdt, P. Lognonné, D. Giardini, S. Ceylan, M. Drilleau, A. C. Duran, R. F. Garcia, Q. Huang, *et al.* (2021). Seismic detection of the martian core, *Science* **373,** no. 6553, 443–448.

Tanaka, K. L., J. A. Skinner, J. M. Dohm, R. P. Irwin, E. J. Kolb, C. M. Fortezzo, T. Platz, G. G. Michael, and T. M. Hare (2014). Geologic map of mars, *U.S. Geol. Surv. Geol. Investig.*, 3292–3292, doi: 10.3133/sim3292.

van Driel, M., S. Ceylan, J. F. Clinton, D. Giardini, A. Horleston, L. Margerin, S. C. Stähler, M. Böse, C. Charalambous, T. Kawamura, *et al.* (2021). High-frequency seismic events on Mars observed by InSight, *J. Geophys. Res.* **126,** no. 2, e2020JE006670, doi: 10.1029/2020JE006670.

Weber, R. C., P.-Y. Lin, E. J. Garnero, Q. Williams, and P. Lognonné (2011). Seismic detection of the lunar core, *Science* **331,** no. 6015, 309–312.

Authors and Affiliations

Anna C. Horleston: School of Earth Sciences, University of Bristol, Bristol, United Kingdom, https://orcid.org/0000-0002-6748-6522; **John F. Clinton:** Swiss Seismological Service, ETH Zürich, Zürich, Switzerland, https://orcid.org/0000-0001-8626-2703; **Savas Ceylan:** Institute of Geophysics, ETH Zürich, Zürich, Switzerland, https://orcid.org/0000-0002-6552-6850; **Domenico Giardini:** Institute of Geophysics, ETH Zürich, Zürich, Switzerland, https://orcid.org/0000-0002-5573-7638; **Constantinos Charalambous:** Department of Electrical and Electronic Engineering, Imperial College London, London, United Kingdom, https://orcid.org/0000-0002-9139-3895; **Jessica C. E. Irving:** School of Earth Sciences, University of Bristol, Bristol, United Kingdom, https://orcid.org/0000-0002-0866-8246; **Philippe Lognonné:** Université de Paris, Institut de physique du globe de Paris, CNRS, Paris, France, https://orcid.org/0000-0002-1014-920X; **Simon C. Stähler:** Institute of Geophysics, ETH Zürich, Zürich, Switzerland, https://orcid.org/0000-0002-0783-2489; **Géraldine Zenhäusern:** Institute of Geophysics, ETH Zürich, Zürich, Switzerland, https://orcid.org/0000-0001-9401-4910; **Nikolaj L. Dahmen:** Institute of Geophysics, ETH Zürich, Zürich, Switzerland, https://orcid.org/0000-0002-9114-6747; **Cecilia Duran:** Institute of Geophysics, ETH Zürich, Zürich, Switzerland, https://orcid.org/0000-0003-4269-930X; **Taichi Kawamura:** Université de Paris, Institut de physique du globe de Paris, CNRS, Paris, France, https://orcid.org/0000-0001-5246-5561; **Amir Khan:** Institute of Geophysics, ETH Zürich, Zürich, Switzerland; Physik-Institut, University of Zürich, Zürich, Switzerland, https://orcid.org/0000-0002-7787-4836; **Doyeon Kim:** Institute of Geophysics, ETH Zürich, Zürich, Switzerland, https://orcid.org/0000-0003-4594-2336; **Matthieu Plasman:** Université de Paris, Institut de physique du globe de Paris, CNRS, Paris, France, https://orcid.org/0000-0002-5630-2089; **Fabian Euchner:** Institute of Geophysics, ETH Zürich, Zürich, Switzerland, https://orcid.org/0000-0001-6340-7439; **Caroline Beghein:** Department of Earth, Planetary, and Space Sciences, University of California, Los Angeles, California, U.S.A., https://orcid.org/0000-0002-3158-2213; **Éric Beucler:** Laboratoire de Planétologie et Géodynamique, Univ. Nantes, Univ. Angers, CNRS, Nantes, France, https://orcid.org/0000-0003-2605-4990; **Quancheng Huang:** Department of Geophysics, Colorado School of Mines, Golden, Colorado, U.S.A., https://orcid.org/0000-0002-5681-5159; **Martin Knapmeyer:** DLR Institute of Planetary Research, Berlin, Germany, https://orcid.org/0000-0003-0319-2514; **Brigitte Knapmeyer-Endrun:** Bensberg Observatory, University of Cologne, Bergisch Gladbach, Germany, https://orcid.org/0000-0003-3309-6785; **Vedran Lekić:** Department of Geology, University of Maryland, College Park, Maryland, U.S.A., https://orcid.org/0000-0002-3548-272X; **Jiaqi Li:** Department of Earth, Planetary, and Space Sciences, University of California, Los Angeles, California, U.S.A., https://orcid.org/0000-0001-7525-5401; **Clément Perrin:** Laboratoire de Planétologie et Géodynamique, Univ. Nantes, Univ. Angers, CNRS, Nantes, France, https://orcid.org/0000-0002-7200-5682; **Martin Schimmel:** Geosciences Barcelona—CSIC, Barcelona, Spain, https://orcid.org/0000-0003-2601-4462; **Nicholas C. Schmerr:** Department of Geology, University of Maryland, College Park, Maryland, U.S.A., https://orcid.org/0000-0002-3256-1262; **Alexander E. Stott:** Institut Supérieur de

l'Aéronautique et de l'Espace SUPAERO, Toulouse, France, https://orcid.org/0000-0001-6121-705X; **Eléonore Stutzmann:** Université de Paris, Institut de physique du globe de Paris, CNRS, Paris, France, https://orcid.org/0000-0002-4348-7475; **Nicholas A. Teanby:** School of Earth Sciences, University of Bristol, Bristol, United Kingdom, https://orcid.org/0000-0003-3108-5775; **Zongbo Xu:** Université de Paris, Institut de physique du globe de Paris, CNRS, Paris, France, https://orcid.org/0000-0002-5670-6761; **Mark Panning:** Jet Propulsion Laboratory, California Institute of Technology, Pasadena, California, U.S.A., https://orcid.org/0000-0002-2041-3190; and **William B. Banerdt:** Jet Propulsion Laboratory, California Institute of Technology, Pasadena, California, U.S.A., https://orcid.org/0000-0003-3125-1542

Manuscript received 11 February 2022
Published online 22 April 2022